

FINITE ELEMENT SIMULATION OF HIGH SPEED MACHINING Ti-6Al-4V ALLOY USING MODIFIED MATERIAL MODELS

Tuğrul Özel and Mohammad Sima
Manufacturing Automation Research Laboratory
Department of Industrial and Systems Engineering
Rutgers University
Piscataway, New Jersey

Anil K. Srivastava
TechSolve Inc.
Cincinnati, Ohio

KEYWORDS

Finite Element Analysis, titanium alloys, and machining.

ABSTRACT

Titanium alloys present superior properties such as high strength-to-weight ratio and resistance to corrosion but possess poor machinability. Finite element simulations can be used to study the influence of process parameters. In this work, constitutive material models are modified to simulate serrated chip formation which can be extended to other materials. In modified models, strain (flow) softening, strain hardening and thermal softening effects are coupled. The predictions are compared with orthogonal cutting tests and found to be in agreement.

INTRODUCTION

Titanium alloys such as Ti-6Al-4V offer high strength-to-weight ratio, high toughness, superb corrosion resistance, and bio-compatibility and are increasingly used in aerospace and biomedical applications. However, titanium alloys are difficult to machine due to their low thermal conductivity and diffusivity, high rigidity and low elasticity modulus and high chemical reactivity at elevated temperatures. Extensive studies have been reported with focus on serrated chip formation mechanism (Komanduri and von Turkovich 1981, Xie et al. 1996, Barry et al. 2001, Cotterell and Byrne 2008), adiabatic shear band modeling (Komanduri and Zhu 2002,

Shivpuri et al. 2002, Baeker et al. 2002, Calamaz et al. 2008), and tool wear (Kitagawa et al. 1997, Zoya and Krishnamurthy 2000, Corduan et al. 2003). Quick-stop experiments are often used to capture instantaneous chip formation (see Fig.1). Such chip pictures depict highly serrated shape with regions of co-existing adiabatic shear bands and cracks. These segmented, but continuous, chips are often formed at high cutting speeds. Adiabatic shear bands, a form of failure mechanism and the precursors to fracture, occur in titanium alloys, are usually very narrow (5-500 μm) and they consist of highly sheared material.

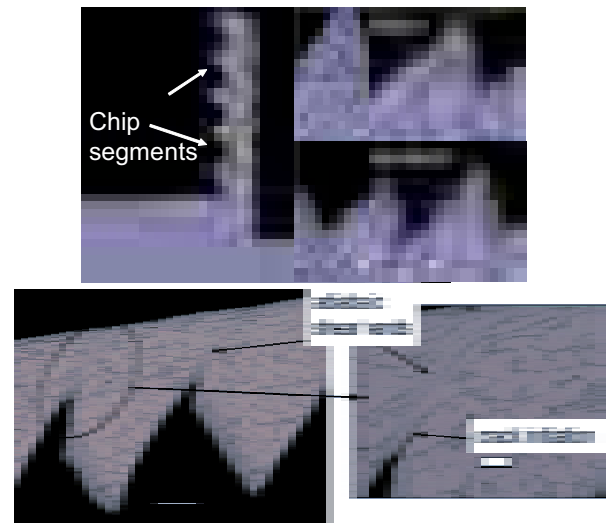


FIGURE 1: IMAGES OF CHIP FORMATION IN ORTHOGONAL CUTTING OF Ti-6Al-4V (BAEKER ET AL, 2002; CALAMAZ ET AL. 2008).

Generally, chip load and cutting speed for machining titanium alloys are kept low to avoid excessive heat generation. Usually above 120 m/min is considered the high-speed machining range for titanium alloys. However, due to low thermal conductivity cutting temperatures can reach well above 1000 °C during machining. Titanium material undergoes phase transformation between 800 and 850 °C from an h.c.p (known as α -Ti) to a b.c.c. structure (known as β -Ti) at which a more slip system exists, thereby contributing to adiabatic shearing and forming of serrated chips (Shivpuri et al. 2002). Finite element models are often utilized to investigate the serrated chip formation in machining of titanium alloys (Li and Shih 2007). It is possible to explain the serrated chip formation using only damage models (Obikawa and Usui 1996, Baeker et al. 2002, Shivpuri et al. 2002), adiabatic shearing (Calamaz et al. 2008) or both (Ozel et al. 2009). The influence of serrated chip formation on machining process outputs (cutting forces, temperature and surface roughness and integrity) is profound. Therefore, a thorough understanding of mechanics of serrated chip formation is important. This work aims to investigate the influence of material modeling for serrate chip formation in Ti-6Al-4V alloy using finite element simulations.

EXPERIMENTAL WORK

Orthogonal turning of Ti-6Al-4V titanium alloy tubes (50.8 mm diameter and 3.175 mm thick) have been performed using uncoated tungsten carbide (WC/Co) cutting tools in a rigid CNC turning centre at TechSolve Inc. The cutting forces were measured with a force dynamometer and high-speed data acquisition devices. The experiments have been conducted using uncoated carbide tools with sharp edges with 0° rake angle (γ) at two different cutting speed ($V=120, 240$ m/min) and five different uncut chip thickness ($t_c=0.0254, 0.0508, 0.0762, 0.1016, 0.127$ mm). Cutting forces measured in orthogonal cutting tests of Ti-6Al-4V alloy tubes have been presented in Fig. 2.

CONSTITUTIVE MATERIAL MODELS

Most commonly used material models include the Johnson-Cook material model (Johnson and Cook 1983), Baumann-Chiesa-Johnson (BCJ) model (Bammann et al. 1996) and the Nemat-Nasser model (Nemat-Nasser et al. 2001). These models for the dynamic material behavior

are often obtained by using Split Hopkinson bar tests and offer data at much lower levels of strain (up to 0.3 mm/mm) and strain-rates (up to 10^3 s⁻¹) than the ones observed at shear zones in machining. The data is extrapolated to the ranges in machining and utilized in finite element modeling.

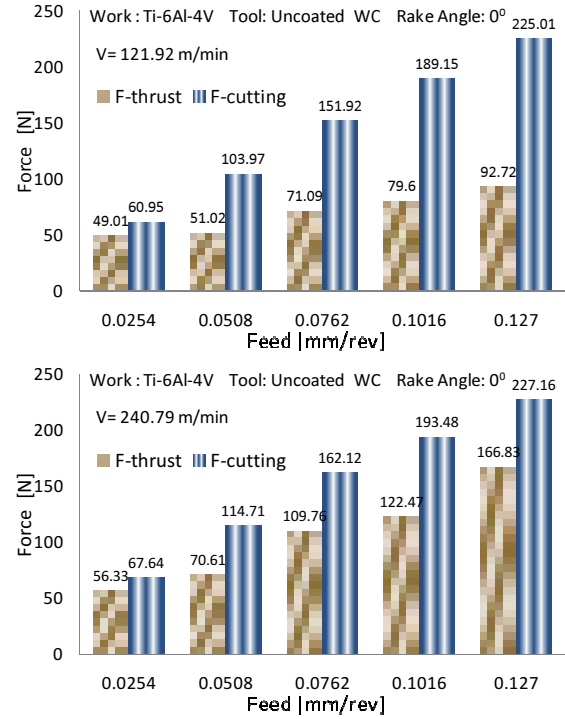


FIGURE 2: FORCES IN MACHINING Ti-6Al-4V.

The Johnson-Cook model

Three different Johnson-Cook material models for Ti-6Al-4V titanium alloy are considered. Table 1 shows parameters of the Johnson-Cook (JC) constitutive equation for Ti-6Al-4V for each model.

$$\bar{\sigma} = \left[A + B(\epsilon)^n \right] \left[1 + C \ln \left(\frac{\dot{\epsilon}}{\dot{\epsilon}_0} \right) \right] \left[1 - \left(\frac{T - T_0}{T_m - T_0} \right)^m \right] \quad (1)$$

In Eq. (1) the parameter A is the initial yield strength of the material at room temperature. The equivalent plastic strain rate $\dot{\epsilon}$ is normalized with a reference strain rate $\dot{\epsilon}_0$. T_0 is room temperature, and T_m is the melting temperature of the material (1604 °C). The parameter n takes into account the strain hardening effect, the parameter m models the thermal softening effect, and C represents strain rate sensitivity.

TABLE 1: CONSTANTS OF J-C MODEL FOR TI-6AL-4V.

Model	A	B	C	n	m
Lee-Lin	782.7	498.4	0.028	0.28	1.0
Meyer-Kleponis	862.5	331.2	0.012	0.34	0.8
Kay	1098	1092	0.014	0.93	1.1

The J-C model constants shown in Table 2 are obtained at different testing conditions. Lee and Lin (1998) obtained them at a constant strain rate of 2000 s^{-1} and a maximum true strain of 0.3 mm/mm . Meyer and Kleponis (2001) used strain rate levels of 0.0001 s^{-1} , 0.1 s^{-1} and 2150 s^{-1} and a maximum plastic strain of 0.57 mm/mm . Kay (2003) tested under strains up to 0.6 mm/mm and strain rates up to 10^4 s^{-1} .

Modified Johnson-Cook models

Recently reported studies offered modified material models that include strain (flow) softening phenomenon (Shivpuri et al. 2002, Baeker et al. 2002, Calamaz et al. 2008, Anurag and Guo 2007, Özel et al. 2009, Karpal 2009). Localized strain softening phenomenon can be described as offering less resistance to local plastic deformations due to rearrangement of dislocations caused by subsequent cycling in hard materials. This phenomenon is usually seen during an increase in strain beyond a critical strain value.

During strain softening, flow stress begins to decrease with increasing strain beyond a critical strain value and resumes strain hardening behavior with further increase in strain. Below that critical strain, the material exhibits strain hardening. The strain softening modification can be included in the modified J-C flow stress model as following:

Model 1: A modified J-C model that includes strain softening effect using an overarching modifier that consists a \tanh function which leaves flow stress at low (experimental) strains unchanged and introduce different levels of softening at higher strains through parameters p , r , s , and M is introduced (Eq. 2).

$$\sigma = [A + B\varepsilon^n] \left[1 + C \ln \frac{\dot{\varepsilon}}{\dot{\varepsilon}_0} \right] \left[1 - \left(\frac{T - T_r}{T_m - T_r} \right)^m \right] \left[M + (1 - M) \left[\tanh \left(\frac{1}{(\varepsilon + p)^r} \right) \right]^s \right] \quad (2)$$

Model 2: Modifications to the thermal softening part of the J-C model by including temperature dependent strain softening are proposed and the model is given in Eq.(3).

$$\sigma = [A + B\varepsilon^n] \left[1 + C \ln \frac{\dot{\varepsilon}}{\dot{\varepsilon}_0} \right] \left[1 - \left(\frac{T - T_r}{T_m - T_r} \right)^m \right] \left[D + (1 - D) \left[\tanh \left(\frac{1}{(\varepsilon + p)^r} \right) \right]^s \right] \quad (3)$$

Model 3: Further modifications to the strain hardening part of the J-C model by including strain softening at higher strain values are proposed and the model is given in Eq. (4).

$$\sigma = \left[A + B\varepsilon^n \left(\frac{1}{\exp(\varepsilon^a)} \right) \right] \left[1 + C \ln \frac{\dot{\varepsilon}}{\dot{\varepsilon}_0} \right] \left[1 - \left(\frac{T - T_r}{T_m - T_r} \right)^m \right] \left[D + (1 - D) \left[\tanh \left(\frac{1}{(\varepsilon + p)^r} \right) \right]^s \right] \quad (4)$$

where $D = 1 - \left(\frac{T}{T_m} \right)^d$, and $p = \left(\frac{T}{T_m} \right)^b$.

The experimental flow stress data by Lee and Lin (1998) has been taken as the base Johnson-Cook model.

For Model 1, the parameters p and r are taken as $p=0$ and $r=1$. The effect of strain softening is presented in Fig. 3. The parameter M substantially modifies the flow stress after a critical value of strain around 0.5 mm/mm .

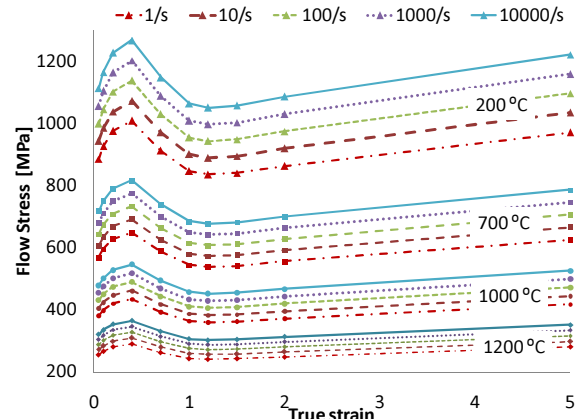


FIGURE 3: FLOW STRESS CURVES WITH STRAIN SOFTENING $M=7$, $s=7$ (MODEL 1).

FINITE ELEMENT SIMULATIONS

In this study, finite element model is developed using updated Lagrangian software in which chip separation from workpiece is achieved with continuous remeshing. Two sets of finite

element simulations are considered; (a) coupled thermo viscoplastic and (b) elasto-viscoplastic.

The viscoplastic simulations included a workpiece as viscoplastic with a mesh containing 8000 quadrilateral elements. PcBN tool is modeled as rigid with a mesh containing into 2000 elements. A rake angle (γ) of 0° and a tool edge radius (r_β) of $40 \mu\text{m}$ are employed in the tool geometry. These models are compared with experimental results from Zoya and Krishnamurthy (2000).

The elasto-viscoplastic simulations included a workpiece as elasto-viscoplastic with a mesh containing 10000 quadrilateral elements. Uncoated carbide tool is modeled as rigid with a mesh containing into 2500 elements. A rake angle (γ) of 0° and a tool edge radius (r_β) of $5 \mu\text{m}$ are employed in the tool geometry. These simulation models are compared with experimental results obtained in this study.

A plane-strain coupled thermo-mechanical analysis was performed using orthogonal cutting assumption. Thermal boundary conditions are defined accordingly in order to allow heat transfer from workpiece to cutting tool. The heat conduction coefficient (h) is taken as $1000 \text{ kW.m}^{-2} \text{ K}^{-1}$ to allow rapid temperature rise in the tool. Mechanical and thermo-physical properties of titanium Ti-6Al-4V alloy are defined as temperature (T) dependent. Temperature-dependent (T in $^\circ\text{C}$) Young's modulus (E), thermal expansion (α), thermal conductivity (λ), heat capacity (c_p) is defined as below:

$$E(T) = 0.7412 \cdot T + 113375 \quad [\text{MPa}] \quad (4)$$

$$\alpha(T) = 3.10^{-9} \cdot T + 7.10^{-6} \quad [\text{mm.mm}^{-1} \cdot ^\circ\text{C}^{-1}] \quad (5)$$

$$\lambda(T) = 7.039e^{0.0011 \cdot T} \quad [\text{W.m}^{-1} \cdot ^\circ\text{C}^{-1}] \quad (6)$$

$$C_p(T) = 2.24e^{0.0007 \cdot T} \quad [\text{N.mm}^{-2} \cdot ^\circ\text{C}^{-1}] \quad (7)$$

Chip-tool interfacial friction model

The friction in machining is indeed complex and requires use of variable friction along the edge radius and rake face of the insert. Friction factor, which is defined as $m = \tau/k$ where τ is frictional shear stress and k is the work material shear flow stress, is commonly used at severe contact conditions. Whereas a Coulomb friction coefficient is applied to mild contact conditions. Friction along the tool rake face when curvilinear (round or waterfall-oval) edge inserts are employed is more sophisticated. According to rake

face friction factor identification results by Karpat and Özel (2008), friction factor decreases with increasing ratio of uncut chip thickness to edge radius and increasing cutting speed. Three distinct regions are recommended for the chip-tool interfacial friction.

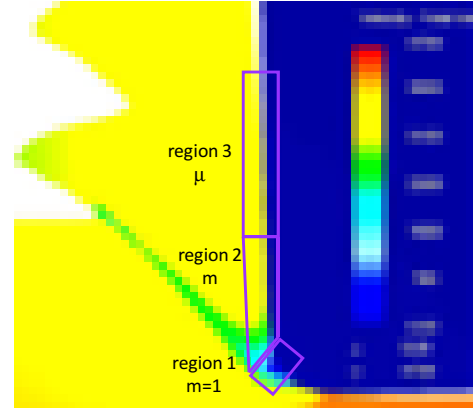


FIGURE 4: VELOCITY FIELD AND FRICTION REGIONS.

In this paper, three friction regions are considered: (i) shear friction $m=1$ from the tool tip point to the end of the tool edge curvature, (ii) a constant shear friction from the end of the curvature to the uncut chip thickness boundary on the rake face, (iii) a coefficient of friction along the rake face from the boundary of the uncut chip thickness to the end point of chip-tool contact as shown in Fig.4. Parameters for the friction models used in FE simulations are given in Table 2.

Fracture criterion

As it will be presented here, the simulation of chip segmentation in machining titanium alloys can be offered either by using a damage related crack initiation and propagation together with viscoplastic formulation or by using adiabatic shearing based on strain (flow) softening elasto-viscoplastic work material assumption.

The chip segmentation based on crack initiation and propagation can be modeled using the Cockroft and Latham (1968) (C-L) damage criterion. According to C-L criterion damage occurs when accumulated stress state over the plastic strain reaches to a critical damage value (D_{cr}) as given below.

$$D = \int_0^{\bar{\epsilon}_f} \sigma_1 d\bar{\epsilon} \quad (8)$$

where $\bar{\epsilon}_f$ is the effective fracture strain and σ_1 is the maximum principal stress. Therefore, chip segmentation begins where the damage expression reaches to a critical damage value ($D=D_{cr}$).

TABLE 2: SIMULATION CONDITIONS

V [m/min]	t_u [mm]	Reg.1 (m)	Reg.2 (m)	Reg.3 (μ)	D_{cr}
280	0.10	1	0.70	0.5	90
280	0.05	1	0.70	0.5	90
220	0.10	1	0.75	0.5	90
220	0.05	1	0.75	0.5	90
185	0.10	1	0.80	0.5	90
185	0.05	1	0.80	0.5	120

Viscoplastic Simulations with Damage Criterion

Formation of serrated chips is simulated from the incipient to the steady-state using a damage model. At the beginning cutting, mechanics is very similar to continuous chip formation. A main shear angle forms, then this plane becomes a band as adiabatic shearing takes place. Outer surface of the workpiece bulges during an upsetting phase and an inclination angle forms which becomes the base for the pitch of the serration (Cotterell and Byrne 2008).

In the meantime, local stress-strain state results in critical damage in which a crack is initiated as shown in Fig.5. Depending on the severity of the cutting conditions, crack may deepen and high strain root of a segment forms. Cutting forces predicted are compared with the experimental results from the work by Zoya and Krishnamurthy (2000) at a feed of 0.05 mm as shown in Fig. 6. Predicted chip formation images with the increase in feed and cutting speed is given in a map as shown in Fig. 7. Based on these results, J-C models by Lee and Lin (1998) and Meyer and Kleponis (2001) are found close. Localized shearing due to thermal softening is not so evident since the temperatures predicted are around 400 °C in the chip segments which is lower than allotropic (phase) transformation temperature of Ti-6Al-4V alloy. At higher cutting speeds, localized shearing is expected to be more dominant in serrated chip formation mechanism. The results also reveal that material flow stress greatly affects not only chip formation

mechanism but also forces and temperatures predicted.

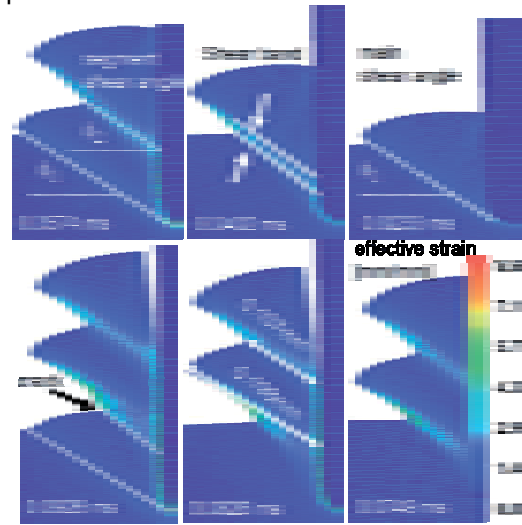


FIGURE 5: SERRATED CHIP FORMATION SIMULATED ($V=280$ m/min, $t_u=0.10$ mm).

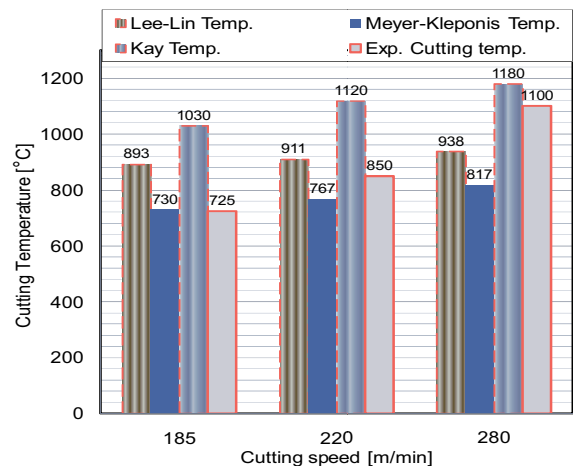
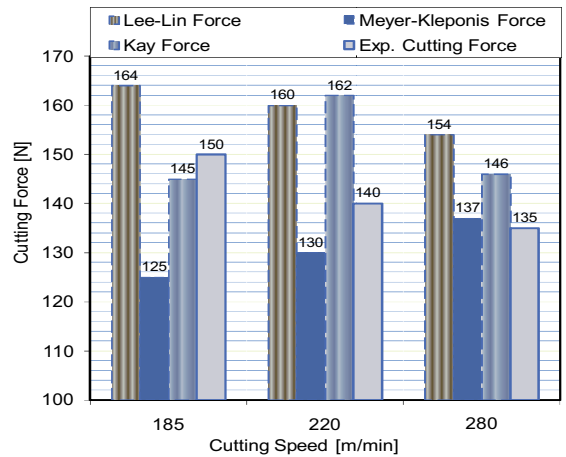


FIGURE 6: COMPARISON OF FORCES AND TEMPERATURES.

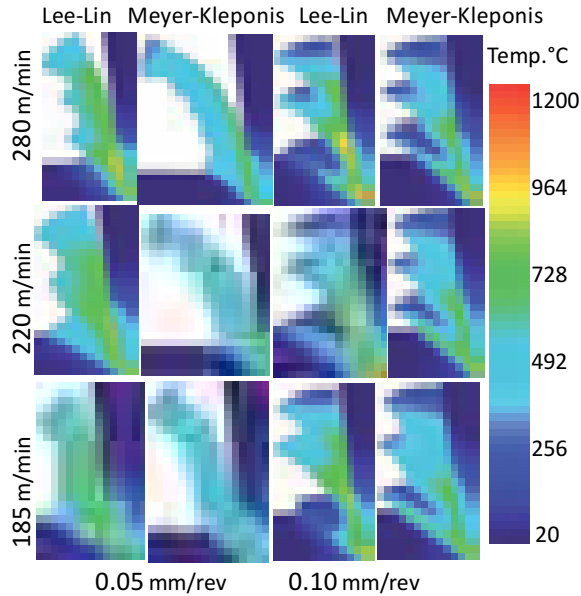


FIGURE 7: SIMULATED SERRATED CHIP FORMATION.

Elasto-Viscoplastic Simulations without Damage Criterion

In these simulations, serrated chip formation process is simulated from the incipient to the steady-state by using adiabatic shearing based on strain (flow) softening elasto-viscoplastic work material assumption. A set of simulations for benchmarking the modified J-C models (Model 1, Model 2, Model 3) is conducted with conditions summarized in Table 3.

TABLE 3: SIMULATION CONDITIONS

V [m/min]	t_u [mm]	Reg.1 (m)	Reg.2 (m)	Reg.3 (μ)
120	0.075	1	0.85	0.5
120	0.100	1	0.80	0.5
120	0.125	1	0.75	0.5

Influence of modified J-C model (Model1) parameters on the serrated chip formation can be seen in Fig.8.

After several iterations, the model parameters shown in Table 4 are chosen as the most suitable parameters to modify J-C material model without changing the Lee and Lin (1998) Split-Hopkinson bar test data which are mostly obtained at lower strains.

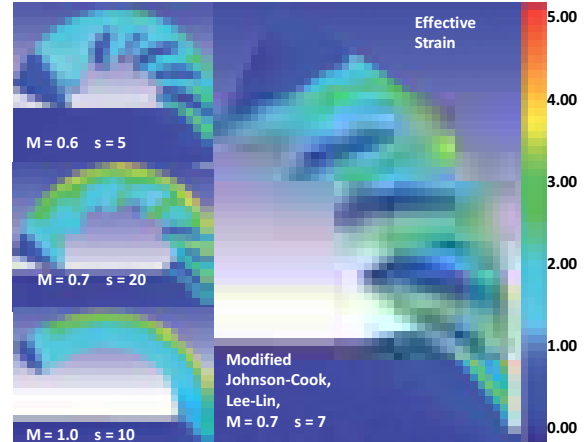


FIGURE 8: SERRATED CHIP FORMATION WITH ADIABATIC SHEARING USING MODEL 1 ($V = 120$ m/min, $t_u = 0.1$ mm/rev, 0° rake angle, $r_\beta = 5 \mu\text{m}$).

Several modified J-C models are tested against each other at the same cutting condition ($V = 120$ m/min, $t_u = 0.1$ mm/rev, 0° rake angle, $r_\beta = 5$ mm) and predicted forces are compared with the experimentally measured cutting (F_c) and thrust (F_t) forces as shown in Fig. 9. Thus experimental data reported in this study have been used to validate the elasto-viscoplastic finite element simulations. Since influence of friction conditions on the simulation results is not the focus of this study, same friction parameters given in Table 3 have been applied to simulations with different modified J-C models.

TABLE 4: PARAMETERS OF THE MODIFIED J-C MODELS

	M	s	a	b	r	d
Model 1	0.7	4	-	-	-	-
Model 2	-	1.5	-	2	2	1
Model 3	-	0.05	2	5	2	1

Predictions obtained with simulations using Model 3 have resulted in closest matches to the experimental forces. Therefore, this modified J-C material model is adapted as the flow stress for the simulation of machining Ti-6Al-4V alloy. The model has also resulted in close matches in cutting and thrust forces for the two other uncut chip thickness conditions as shown in Fig. 10.

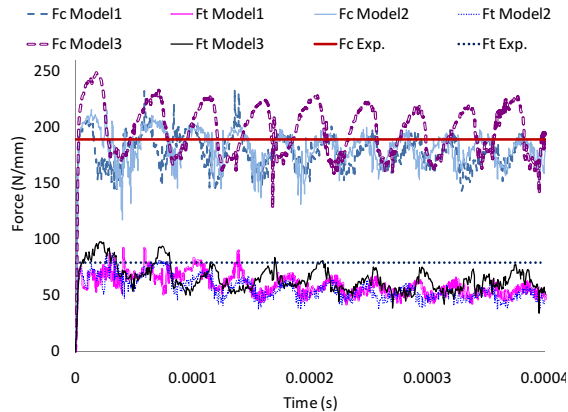


FIGURE 9: COMPARISON OF FORCES PREDICTED ($V=120$ m/min, $t_u=0.1$ mm/rev, 0° rake angle, $r_\beta=5$ mm).

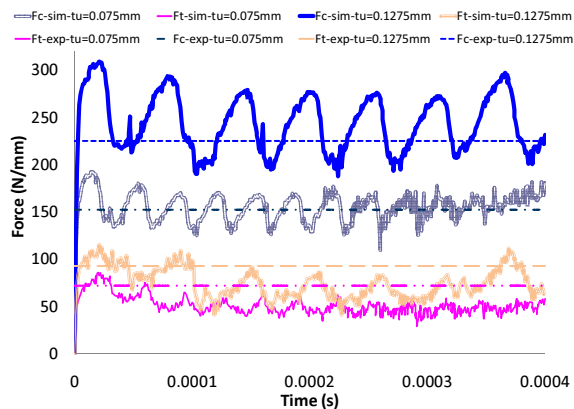


FIGURE 10: COMPARISON OF FORCES PREDICTED WITH MODEL 3 ($V=120$ m/min, 0° rake angle, $r_\beta=5$ mm).

As it can be seen from the predicted serrated chips with finite element simulations, a large chip segment (tooth) is followed by a smaller one in almost all models similar to the observations reported by Calamaz et al. (2008). However, the difference is more visible in elasto-viscoplastic simulations using Model 3 in Fig. 11.

The effective strain distributions shown in Fig. 11 show the adiabatic shear bands very clearly. In these simulations no damage criterion was used at all. Fig. 11 also shows the chip morphology for three different uncut chip thickness ($t_u=0.075$, 0.100 , and 0.125 mm).

The geometry and dimensions of the serrated chips are also found very close to the chips reported in Calamaz et al. (2008). The force predictions have been improved by implementing variable friction definition with three distinct regions (sticking and slipping).

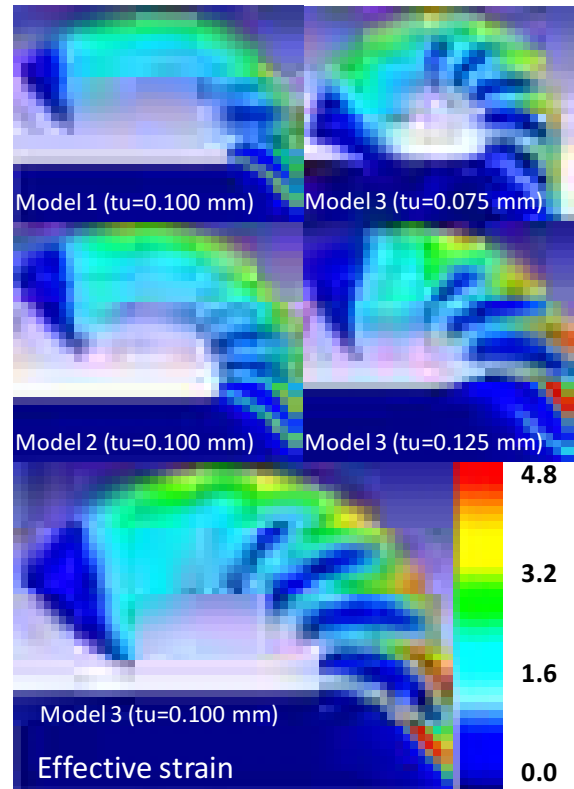


FIGURE 11: SERRATED CHIP FORMATION WITH ADIABATIC SHEARING ($V=120$ m/min, $t_u=0.1$ mm/rev, 0° rake angle, $r_\beta=5$ mm).

CONCLUSIONS

In this study, influence of material constitutive models and finite element formulation on serrated chip formation for modeling of machining Ti-6Al-4V titanium alloy is investigated. Modified material models are used where strain (flow) softening phenomenon, strain hardening and thermal softening effects are coupled. Orthogonal cutting experiments have been conducted with uncoated carbide tools. Finite Element simulations are validated with experimental results using measured cutting forces and chip morphology. The results reveal that material flow stress and finite element formulation greatly affects not only chip formation mechanism but also forces and temperatures predicted. Both localized adiabatic shearing and crack development are active mechanism in machining Ti-6Al-4V alloys.

ACKNOWLEDGEMENTS

The support for this project by the National Science Foundation (CMMI-0758820 and CMMI-0757954) is gratefully acknowledged.

REFERENCES

- Anurag, S., Guo, Y.-B., 2007, A modified micromechanical approach to determine flow stress of work materials experiencing complex deformation histories in manufacturing processes, *International Journal of Mechanical Sciences*, Volume 49/7, 909-918
- Baeker, M., Roesler, J., Siemers, C., 2002, Finite element simulation of segmented chip formation of Ti6Al4V, *ASME J. Manuf. Sci. Eng.* 124:485-488.
- Bammann, D.-J., Chiesa, M.-L., Johnson, G.-C., 1996, Modeling large deformation and failure in manufacturing processes, *Theoretical and Applied Mechanics*, 359–76.
- Barry, J., Byrne, G., Lennon, D., 2001, Observations on chip formation and acoustic emission in machining Ti-6Al-4V alloy, *Int. J. Mach. Tools Manuf.* 41:1055-1070.
- Calamaz, M., Coupard, D., Girot, F., 2008, A new material model for 2D numerical simulation of serrated chip formation when machining titanium alloy Ti-6Al-4V, *International Journal of Machine Tools & Manufacture*, 48, 275–288.
- Cockcroft, M.G., Latham, D.J., 1968, Ductility and the workability of metals, *J. Inst. Met.* 96, 33–39.
- Corduan, N., Himbart, T., Poulachon, G., Dessoly, M., Lambertin, M., Vigneau, J., Poyoux, B., 2003, Wear mechanisms of new tool materials for Ti-6Al-4V high performance machining, *Ann. CIRP.* 52/1:73-76.
- Cotterell, M., Byrne, G., 2008, Dynamics of chip formation during orthogonal cutting of titanium alloy Ti-6Al-4V, *Ann. CIRP*, 57:93-96.
- Johnson, G.R., Cook, W.H., 1983, A constitutive model and data for metals subjected to large strains, high strain rates and high temperature, *Proc. 7th Int. Symp. Ballistics*, The Hague, Netherlands, 541-547.
- Karpat, Y., 2009, Finite element modelling of machining Ti-6Al-4V alloy using a modified material model, *12th CIRP Conference on Modelling of Machining Operations*, pp. 107-114.
- Karpat, Y., Özel, T., 2008, Mechanics of high speed cutting with curvilinear edge tools, *Int. J. Mach. Tools Manuf.* 48:195-208.
- Kay, G., 2003, Failure Modelling of Titanium 6Al-4V and Aluminum 2024-T3 with the Johnson-Cook Material Model, *U.S. Lawrence Livermore Nat. Lab. Rep. DOT/FAA/AR-03/57*.
- Kitagawa, T., Kubo, A., Maekawa, K., 1997, Temperature and Wear of Cutting Tools in High-Speed Machining of Inconel 718 and Ti-6Al-6V-2Sn, *Wear*, 202:142-148.
- Komanduri, R., Hou, Z.B., 2002, On thermoplastic shear instability in the machining of a titanium alloy, *Metall. Mater. Trans. A*, 33A:2995-3010.
- Komanduri, R., von Turkovich, B.F., 1981, New observations on the mechanism of chip formation when machining titanium alloys, *Wear*, 179-188.
- Lee, W. S., Lin, C.F., 1998, High-temperature deformation behavior of Ti6Al4V alloy evaluated by high strain-rate compression tests, *J. Mater. Process. Technol.*, 75:27–136.
- Li, R., Shih, A., 2007, Finite Element Modeling of High-Throughput Drilling of Ti-6Al-4V, *Transactions of NAMRI/SME*, 35:73:80.
- Meyer, H.W., Kleponis, D.S., 2001, Modeling the high strain rate behavior of titanium undergoing ballistic impact and penetration, *Int. J. Impact Eng.* 26:509-521.
- Nemat-Nasser, S., Guo, W-G., Nesterenko, V.F., Indrakanti, S.S., Gu, Y-B., 2001, Dynamic response of conventional and hot isostatically pressed Ti-6Al-4V alloys: experiments and modeling, *Mechanics of Materials*, Vol. 33, pp. 425-439.
- Obikawa, T., Usui, E., 1996, Computational machining of titanium alloy—finite element modeling and a few results, *ASME J. Manuf. Sci. Eng.* 118:208-215.
- Özel, T., Yildiz, S., Ciurana, J., 2009, Influence of Material Models on Serrated Chip Formation in Simulation of Machining Ti-6Al-4V Titanium Alloy, *Proceedings of 12th CIRP Conference on Modeling of Machining Operations*, pp. 123-130.
- Shivpuri, R., Hua, J., Mittal, P., Srivastava, A., 2002, Microstructure-Mechanics Interactions in Modeling Chip Segmentation during Titanium Machining, *Ann. CIRP*, 51:71-74.
- Xie, J.Q., Bayoumi, A.E., Zbib, H.M., 1996, A study on shear banding in chip formation of orthogonal machining, *Int. J. Mach. Tools Manuf.* 36/7:835-847.
- Zoya, Z., Krishnamurthy, R., 2000, The performance of CBN tools in the machining of titanium alloys, *J. Mater. Process. Technol.*, 100:80-86.